Miner Deposita (2012) 47:683–700
DOI 10.1007/s00126-011-0386-z

ARTICLE

The Niujiaotang Cd-rich zinc deposit, Duyun, Guizhou province, southwest China: ore genesis and mechanisms of cadmium concentration

Lin Ye · Nigel J. Cook · Tiegeng Liu · Cristiana L. Ciobanu · Wei Gao · Yulong Yang

Received: 16 September 2010 / Accepted: 5 September 2011 / Published online: 2 October 2011

Abstract The Niujiaotang zinc deposit in southeastern Guizhou, China, is a Mississippi Valley-type Zn deposit within Early Cambrian carbonate rocks. Sphalerite is enriched in cadmium (average 1.4 wt.% Cd), which occurs mostly as isomorphous impurities in the sphalerite lattice. Discrete cadmium minerals (greenockite and otavite) are rare and are found almost exclusively in the oxidation zone of the deposit, probably formed as secondary minerals during weathering–leaching processes. Geochemical data show that the sulfides are enriched in heavy sulfur, with $\delta^{34}S$ ranging from +10.0‰ to +32.8‰ (mean +22.5‰). The consistent Pb isotopic compositions in different sulfide minerals are similar to that of Cambrian strata. The ore lead probably came from U- and Th-rich upper crustal rocks, such as the Lower Cambrian Wuxun Formation. The ore fluid is of low-temperature (101°C to 142°C) type, with a Na–Ca–Mg–Cl-dominant composition, and is interpreted as oil-field brine. The data indicate that the metals were mainly derived from the Early Cambrian strata (Qingxudong and Wuxun Formations), whereas sulfur is sourced from sulfate in Cambrian strata or oil-field brines of the Majiang petroleum paleoreservoir. The genetic model for the deposit invokes an Early Cambrian shallow-sea environment on the Yangtze Platform. Zinc and Cd in seawater were concentrated in abundant algae via unknown biological mechanisms, resulting in large amounts of Zn- and Cd-rich algal ooliths. During the Ordovician, concurrent with destruction of the Majiang petroleum paleoreservoir, oil-field brines migrated from the center of the basin to the margin leaching metals from the Cambrian strata. In the Niujiaotang area, preexisting Zn and Cd, particularly in the Qingxudong and Wuxun Formation, were further mobilized by hot brines rising along the Zaolou fault system, forming stratiform and generally conformable Zn–Cd orebodies in reactive carbonate lithologies.

Keywords Sphalerite · Cadmium · Niujiaotang · China

Editorial handling: B. Lehmann

Electronic supplementary material The online version of this article (doi:10.1007/s00126-011-0386-z) contains supplementary material, which is available to authorized users.

L. Ye (✉) · T. Liu · W. Gao · Y. Yang
State Key Laboratory of Ore Deposit Geochemistry,
Institute of Geochemistry, Chinese Academy of Sciences,
Guiyang 550002, China
e-mail: yelin@vip.gyig.ac.cn

N. J. Cook · C. L. Ciobanu
Centre for Tectonics, Resources and Exploration (TRaX),
School of Earth and Environmental Sciences,
University of Adelaide,
Adelaide, SA 5005, Australia

N. J. Cook
South Australian Museum,
Adelaide, SA, Australia

W. Gao · Y. Yang
Graduate School of Chinese Academy of Sciences,
Beijing 100049, China

Introduction

The crustal abundance of cadmium is estimated at about 0.08 ppm (Rudnick and Gao 2005). A number of independent Cd minerals, such as greenockite, otavite, monteponite, cadmoselite, hawleyite, native cadmium, saukovite, cernyite, and niedermayrite (Vasil'yev 1966; Szymanski 1978; Giester et al. 1998), are known from some deposits, and Cd-bearing varieties of more common sulfide minerals are also known (e.g., Cd-tetrahedrite: Pattrick and Hall 1983,

Cd-freibergite: Pattrick 1978, saukovite: Vasil'yev 1966, and Cd-metacinnabar: Dobbe 1992). Cadmium enrichment has also been noted in phosphorites (Nathan et al. 1977) and in montmorillonite (Di Leo 2000). However, there are no cadmium ore deposits, and Cd is almost exclusively produced as a by-product from mining, smelting, and refining sulfide ores of zinc and, to a lesser degree, lead and copper (Tolcin 2008). Nearly all zinc deposits contain Cd in some amounts, with a mean content of Cd in sphalerite typically between 0.2 and 0.6 wt.% (Liu et al. 1984; Schwartz 2000). The Cd^{2+} tetrahedron has similar covalent/ionic radius and crystal chemical characteristics as Zn^{2+}, so that the two elements may be expected to share comparable geochemical behaviors. Sphalerite (ZnS) is the most economically significant Cd-bearing mineral.

Similar concentrations of Cd are found in ores of different types of Zn–(Pb) ores, including Mississippi Valley-type (MVT) Zn–Pb ores, sedimentary exhalative deposits and volcanogenic massive sulfide deposits. Sphalerite from some MVT, skarn, and epithermal vein deposits may contain significantly higher concentrations of Cd and has accordingly attracted economic interest (Schwartz 2000). Examples of deposits with elevated Cd concentrations include the San Juan mine, Potosi district, Bolivia (Barton and Behre 1954); the Ross mine, Ontario (Chen and Dutrizac 1978); White Pine, Michigan (Brown 1974); Red Dog, Alaska (Kelley et al. 2004); Pb–Zn mines in the Griquatown area, South Africa (Schaefer et al. 2004); Jinding, Yunnan, China (Zhao et al. 2005); Sudbury, Ontario (Cabri et al. 1984); and the Vazante mine, Brazil (Hitzman 2001).

In natural occurrences, FeS has been found to replace ZnS in sphalerite by up to as much as 56 mol% (Barton and Toulmin 1966; Balabin and Urusov 1995; Pattrick et al. 1998). CdS concentrations in sphalerite are definitely lower (<14 mol%, Tauson and Chernyshev 1977; Maurel 1978) and are observed up to 20 mol% only if formed under high-temperature and/or pressure conditions (Tauson and Chernyshev 1977).

Electron microprobe studies have shown that, in some deposits, sphalerite carries Cd concentrations exceeding 1.0 wt.%. Examples include second generation sphalerite in mines of the Rheinisches Schiefergebirge, Germany (2.5 wt.%; Wagner and Cook 1998); 0.7~2.5 wt.% in the Lisheen Pb–Zn deposit, Ireland (Wilkinson and Eyre 2005); 0.5~2.0 wt.% in the epithermal deposits of Kochbulak, Kanimansur, and Zambarak, Uzbekistan (Bortnikov et al. 1995); 2.5 wt.% in Pay Khoy, northern Urals, Russia (Yushkin et al. 1975); >1.0 wt.% with up to 9.0 wt.% in the Ross Mine, Ontario (Chen and Dutrizac 1978); 0.1~1.1 wt.% in Bushy Park (Schaefer et al. 2004); and 1.1 wt.% in Kudriavy volcano, Russia (Chaplygin et al. 2007). Exceptionally high Cd contents in sphalerite have been reported from Bernic Lake, Manitoba (17.6 wt.%; Černý and Harris 1978) and Baisoara, Romania (13.2 wt.%; Cook et al. 2009).

As one of the most important trace elements in sphalerite, the concentration of Cd and its geochemical and genetic significance in Pb–Zn deposits have been the focus of much research (e.g., Liu et al. 1984; Zhang 1987b; Bortnikov et al. 1995; Gottesmann and Kampe 2007; Gottesmann et al. 2009). The environmental behavior of Cd and mitigation of potential hazards of Cd release from the mining of Zn–Pb deposits have also become more and more important in recent years (e.g., Schwartz 2000; Piatak et al. 2004; Järup and Åkesson 2009). In contrast, little work has been done on the mechanisms of primary Cd enrichment and formation of distinctly Cd-enriched deposits.

Sphalerite from Niujiaotang is characteristically enriched in Cd with 1.4 wt.% Cd on average (Ye and Liu 1999). The deposit has resources of over 0.35 Mt Zn and 5.3 kt Cd, i.e., 7.5 Mt @ 19.8% (Chen et al. 1992; Zhang et al. 1994). Lead is present, but at sub-economic grade. Salient aspects of the geology, mineralogy, and environmental aspects of the Niujiaotang deposit have been discussed in a number of papers (Chen et al. 1992; Zhang et al. 1994; Ye and Liu 1997, 1999; Liu and Ye 2000; Liu et al. 2004a, b; Ye 2005; Ye et al. 2005, 2006; Pan et al. 2008). The present paper is, however, the first time this unusual deposit is presented to an English-speaking audience. Research results on the Cd distribution and geochemical features of the deposit allow an improved genetic model to be introduced and discussed.

Geological setting

The Niujiaotang deposit is located in the southern end of the Xiangxi (western Hunan)–Qiandong (eastern Guizhou) Pb–Zn metallogenic belt, at the southeastern margin of the Yangtze Craton, the southern end of the Wangsi anticlinorium, and northwest of the Mandong fault. The belt of mineralization that includes Niujiaotang extends from Yutang in western Hunan Province in the north to Duyun in eastern Guizhou province in the south and is controlled by the NE-trending Shidongkou fault system. The metallogenic belt is about 100 km in length and 20 km in width (Wang 1993; Chen et al. 2005). The belt represents one of the most important Pb–Zn-producing areas of Guizhou and Hunan provinces. Numerous sediment-hosted Pb–Zn deposits have been explored, including Huayuan, Xiunao, Maopo, Zhuping, Yongxi, Wengxi, Yebadong, Longjingjie, Bosong, as well as Niujiaotang (Fig. 1). The orebodies are stratabound, stratiform, and lenticular in shape and typically hosted within dolostones or limestones of Cambrian to Ordovician age. There is no record of magmatic activity in the region.

The basement in Eastern Guizhou province is composed of Late Proterozoic metamorphic volcanic rocks and continental

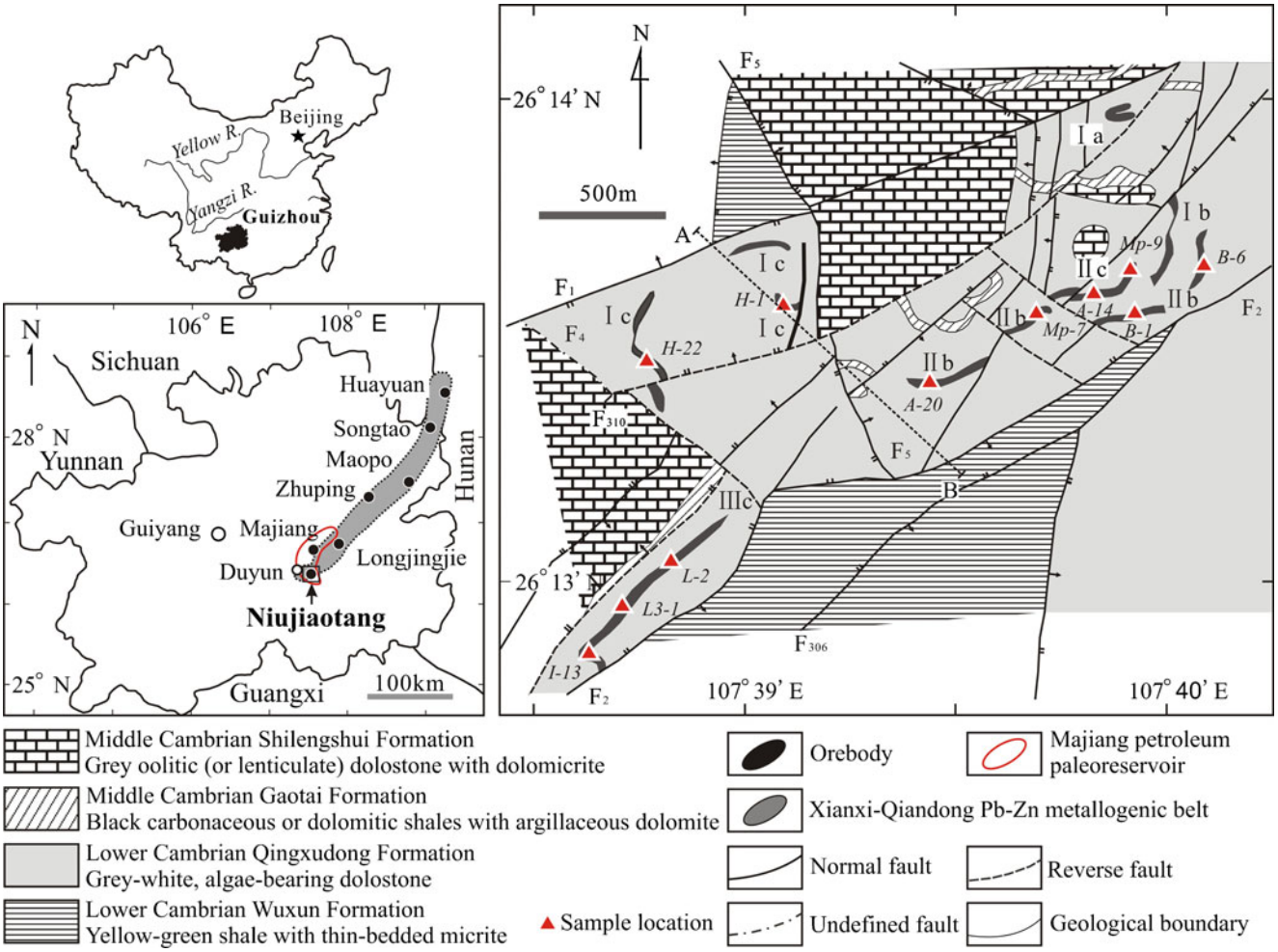

Fig. 1 Geological map of the Niujiaotang deposit (after Chen et al. 1992; Wang and Shi 1997), with individual orebodies and sample locations marked. *Insets* show the location of the deposit within China and the Xianxi–Qiandong metallogenic belt

margin clastic rocks and a >13,000-m-thick Sinian to Middle Triassic marine carbonate series with gentle dip (normally <15°). Strata exposed in the Niujiaotang mining district range from Upper Sinian to Cambrian in age. In order of decreasing age, these formations are as follows: (a) Upper Sinian strata, composed dominantly of carbonate rocks and fine clastic rocks; (b) the Lower Cambrian Wuxun Formation, composed of yellow green shales with thin-bedded micrite, over 150 m in thickness; (c) the Lower Cambrian Qingxudong Formation, which overlies the Lower Cambrian Wuxun Formation—this is the principal ore-hosting sequence at Niujiaotang (Fig. 2) and is predominantly composed of grayish white algae-bearing dolostones, 150~280 m in thickness; (d) the Middle Cambrian Gaotai Formation, composed of black carbonaceous or dolomitic shales with argillaceous dolomite, 10~15 m in thickness; (e) the Middle Cambrian Shilengshui Formation, composed of gray oolitic (or lenticulate) dolostones with dolomicrite, 130~160 m in thickness; and (f) the Middle–Upper Cambrian Loushanguan Group, composed of thick-bedded dolostones, ~1,200 m in thickness. The contact relationships between the rock units of the Cambrian succession, lower Cambrian, and Sinian strata are conformable.

Major faults in the area include the NE-trending Zaolou fault, a subsidiary fault of the NE-trending regional Mandong fault, and its secondary faults. The Zaolou fault, which is composed of a system of parallel NE-trending (40~50°) faults and is characterized by high dip angle (60~75°) and normal fault character, is over 50 km in length and 20~60 m in width with the largest displacement of up to 400 m. Structural research suggests that movement took place in the Ordovician–Silurian Middle–Late Caledonian event (Zhang et al. 1994).

Zinc–Cd mineralization is hosted within algae-bearing dolostones of the Lower Cambrian Qingxudong Formation, which is located at both sides of the secondary faults (e.g., F1 and F2) of the Zaolou fault, showing that ore location is, in part, structurally controlled. Ore is superimposed by a series of NS-, NW-, and EW-trending faults, which formed after mineralization.

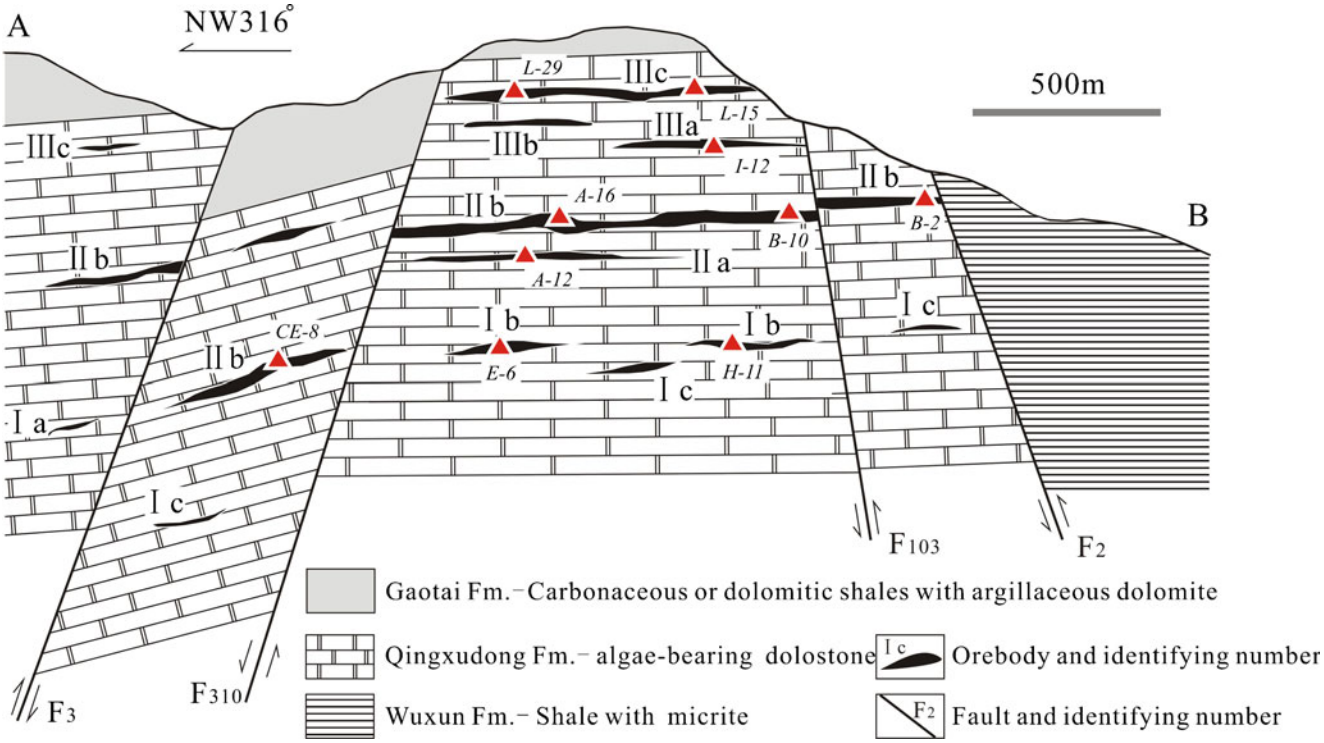

Fig. 2 Cross-section through the Niujiaotang deposit with individual orebodies and sample locations marked (after Chen et al. 1992)

The deposit consists of four sectors. The lenticular, stratabound orebodies are more or less conformable with the surrounding strata (Fig. 2). Orebodies are typically 150~500 m in length and 50~200 m in width, strike NW (310~326°) with low dip angles (15~20°). Among these, the II_b orebody, which is lenticular in shape but locally displays pinch and swell features, is the largest; it is up to 500 m in width and 850 m in length with a thickness varying from 0.3 to 20 m. The grade of the ore is generally within the range of 5.9% to 24.5% Zn and 3,000 to 9,800 ppm Cd with an average value of 19.8 wt.% and 4,081 ppm relatively. The ores can be divided into two types: sulfide ore (sulfide dominant, 75% of reserves) and oxide ore (oxide dominant, 25% of reserves). There is a slightly higher concentration of Cd (479–9,500 ppm, mean 4,282 ppm) in oxide ore than in sulfide ore (539–14,300 ppm, mean 4,012 ppm).

Ore structures are dominated by massive accumulations of sulfide minerals but may also be disseminated and brecciated. The principal ore textures are subhedral–euhedral granular, metasomatic relict texture, metasomatic resorption textures, as well as oolitic, framboidal, bioclast, and microbedding textures. Euhedral–subhedral–anhedral granular textures, metasomatic textures, and framboidal textures are the most common, in which framboidal textures are mainly composed of pyrite with minor sphalerite. Replacement textures are recognized in which sphalerite and galena replace subhedral–euhedral pyrite and sphalerite replaces galena.

The Niujiaotang deposit is located in the southern part of the Majiang petroleum paleoreservoir (Wang and Shi 1997). The original area of this paleoreservoir (Fig. 1 inset) is about 2,450 km^2 with over 1.0 Gt of bitumen (equal to about 1.5 Gt petroleum) in the rocks (Han et al. 1982). Dark black mudstone in the middle–lower part of the Late Cambrian succession is the main hydrocarbon source rock in the district, while the main reservoir rocks are the Late Ordovician carbonate rocks of the Honghuayuan Formation and the second and third members of the Silurian Wongxiang Formation sandstone sequence. The upper part of the Late Ordovician Honghuayuan Formation and Dawan Formation and the fourth member of the Silurian Wongxiang Formation are the main cap rocks (Xiang et al. 2008). Research shows that hydrocarbons began to be generated in the Middle–Late Cambrian and that massive hydrocarbon generation and expulsion took place in the early Ordovician (Xiang et al. 2008; Liu et al. 2009). The trap almost concurrently formed with the peak of the hydrocarbon generation and expulsion, favoring hydrocarbon migration and accumulation. In the Ordovician, when large-scale uplift by the late Caledonian Guangxi tectonic movement took place in the central part of Guizhou Province, the Majiang petroleum paleoreservoir was uplifted and slowly denuded, with escape of liquid hydrocarbon and gradual transformation of oil into bitumen. It is generally believed that the ancient oil and gas reservoir was totally destroyed during this period (Zhang 1987a; Xiang et al. 2008; Liu et al. 2009).

Detailed field and microscopic examinations indicate that the dominant ore minerals in the Niujiaotang deposit form a series of low-temperature mineral associations, including sphalerite and pyrite with minor galena and marcasite, as well as arsenopyrite and stibnite; sphalerite is the most important ore mineral. Gangue mineralogy is dominated by dolomite with subordinate calcite, clay minerals, and quartz. In the oxidation zone, common minerals are smithsonite, hemimorphite, limonite, greenockite, otavite, and some oxides of cadmium. Sphalerite is characteristically fine-grained, subhedral–euhedral granular, and granular in shape (0.02~10 mm). Most sphalerite is light yellow in color; brownish, reddish brown, and black species are occasionally observed. The black or brown sphalerite, pyrite, and galena are usually replaced by light yellow sphalerite. Sometimes, zoned growth textures are seen, with a core zone of black–brown sphalerite enclosed by light yellow sphalerite. Such textures are indicative of a two-stage genesis, the black to brown sphalerite predating the later pale yellow sphalerite. Dolomitization is the dominant style of wallrock alteration close to the ore, followed by pyritization and weak silicification. It is worth pointing out that black bitumen is abundant in nearby orebodies, where it occurs among dolomite grains, in fractured dolostones, and within calcite-dominant geodes. Although not present at Niujiaotang, its presence in the other deposits is taken to imply that the Zn–Cd mineralization is related to bituminization.

Cadmium distribution in the Niujiaotang deposit

Methodology

All analyzed samples were collected from the Mapo nos. II and III ore blocks in the deposit (Figs. 1 and 2). Sulfides (sphalerite, pyrite, galena, etc.) were separated by hand with a purity better than 99% (containing <1% impurities as examined by X-ray diffraction by Gong Guohong, Institute of Geochemistry, Chinese Academy of Sciences (IG-CAS), Guiyang), and ores, dolostones, and sulfides were then fine-ground to <200 mesh (<75 μm). Lead, Zn, Fe, and S were determined by conventional chemical methods; the precision of the method is 0.01 wt.% with an analytical error of 5%. Cadmium, Ag, Ga, and Ge concentrations in ores and the composition of dolostones were determined by atomic absorption spectroscopy (PE-5100-PC) with an analytical error of 2.6%. Minerals were analyzed by electron microprobe (EPMA-1600) with EDAX (Genesis) spectrometer. Instrument conditions were 25 kV accelerating voltage, 20 nA beam current, and 1 μm electron beam spot diameter. Synthetic ZnS, PbS, and Fe_2S standards (SPI) were used. All related analytical processes were made using the method of Tu et al. (2003) and performed at IG-CAS, Guiyang.

Geochemical distribution of Cd in ores

The results of chemical analyses by conventional chemical methods (Table 1, Electronic Appendix A) show that the Cd content of bulk sulfide ores displays wide variation, from 539 to 14,300 ppm with a mean of 4,012 ppm (n=38). The Zn content of the same samples ranges from 4.4 to 28.7 wt.%, with a mean of 16.9 wt.%. The Pb content is rather low, usually <0.1 wt.%. There is a positive correlation between Cd and Zn (Fig. 3) with a correlation coefficient of 0.59. There is, however, no obvious correlation between Cd and Fe or between Cd and Pb (r=−0.23 and −0.21, respectively). This clearly shows that the distribution of Cd, which is dominantly contained within sphalerite, is related to that of Zn in the primary ores. The variation in Cd content of the oxide ores is correspondingly wide, ranging from 479 to 9,500 ppm with an average of 4,639 ppm (n=12, Cd exceeds 3,000 ppm in most oxide ores) (Table 1; Electronic Appendix A), and the Zn content varies between 4.4 and 28.4 wt.% (mean 19.7 wt.%; n=12), remarkably similar to that of primary ores. There is actually a stronger positive correlation (Fig. 3) between Cd and Zn in the oxide ores (correlation coefficient 0.82; n=12). The higher mean concentration of Cd relative to Zn shows that both elements still closely coexist under supergene conditions. In addition to Cd and Zn, concentrations of Ga and Ge also reach grades of economic interest (up to 52 and 58 ppm, respectively), with mean concentrations of 15–17 and 19 ppm in sulfide and oxide ores, respectively (Table 1; Electronic Appendix A).

Mineralogical distribution of Cd in ores

As the most significant Cd-bearing mineral in the deposit, sphalerite is usually rich in Cd and poor in Fe with Zn/Cd ratios varying from 28.2 to 96.4 (mean 55.3; Table 1 and Fig. 4). There are significant differences in the minor element (Cd and Fe) contents of sphalerite of different colors. Black sphalerite is relatively rich in Fe and poor in Cd and Zn (mean Fe 2.3 wt.%, Cd 11,500 ppm, Zn 62.5 wt.%; n=10). Brown sphalerite is poorer in Fe and moderately rich in Cd and Zn (mean Fe 0.90 wt.%, Cd 13,700 ppm, Zn 63.5 wt.%; n=4). Analytical results using atomic absorption spectroscopy and electron microprobe microanalysis show that light yellow sphalerite is impoverished in Fe (0.8 wt.%) and particularly rich in Cd and Zn (mean Cd 15,600 ppm, Zn 65.2 wt.%; n=19), with a Zn/Cd ratio of 44.6. Correlation analysis demonstrates that Zn is positively correlated with Cd (r=0.38; n=33) in all types of sphalerite. Importantly, there is no correlation

Table 1 Summary of geochemical data for bulk ores, host rocks, and sphalerite with different colors and electron probe microanalytical data for light yellow sphalerite and other minerals

Sample	Number of sample	Zn (wt.%)	Cd (ppm)	Fe (wt.%)	Pb (wt.%)	S (wt.%)	Ag (ppm)	Ga (ppm)	Ge (ppm)
Whole rock analysis									
Sulfide ore	38	4.42-28.70 (16.86)	539–14,300 (4,012)	0.32–31.36 (8.32)	0.01–30.88 (3.59)	–	6–52 (15)	4–52 (17)	3–58 (19)
Oxide ore	12	4.42–28.44 (19.67)	479–9,500 (4,639)	6.89–46.05 (18.86)	0.05–0.25 (0.11)	–	5–31 (20)	5–34 (15)	9–55 (19)
Dolostone within ore area	7	0.31–1.57 (0.94)	40–340 (190)	0.22–0.36 (0.30)	0.01–0.02 (0.01)	–	–	2.10–4.50 (2.77)	0.96–3.22 (1.41)
Dolostone outside ore area	10	0.005–0.025 (0.02)	18–42 (30)	0.20–0.33 (0.28)	0–0.01 (0.01)	–	–	1–2.60 (1.90)	0.20–0.91 (0.58)
Black sphalerite	10	54.93–66.62 (62.54)	5,700–17,000 (11,500)	0.78–4.80 (2.31)	0.03–0.10 (0.06)	29.64–33.86 (31.78)	6–18 (12)	–	–
Brown sphalerite	4	62.32–64.70 (63.49)	11,200–15,600 (13,700)	0.82–0.97 (0.90)	0.05–0.08 0.06	30.41–32.46 (31.48)	12–16 (13)	–	–
Light yellow sphalerite	10	62.08–66.36 (64.39)	10,600–19,700 (16,200)	0.35–1.53 (0.88)	0.02–0.13 (0.06)	30.21–34.17 (32.27)	1–73 (41)	1,500[a]	2,900[a]
Electron microprobe data									
Light yellow sphalerite	9	64.57–67.96 (66.14)	8,580–23,350 (15,250)	0.17–1.23 (0.70)	0.02–0.20 (0.14)	31.62–32.86 (32.06)	–	250–1,630 (980)	–
Sphalerite (mean of all)	33	(64.20)	(14,200)	(1.19)	(0.08)	(31.94)		–	–
Pyrite	4	1.43–2.15 (2.79)	183–2,500 (1,345)	40.90–42.11 (41.57)	0.03–0.12 (0.09)	–	–	–	–
Galena	14	0.64–1.89 (1.77)	830–8,685 (3,233)	0.17–0.28 (0.21)	80.53–81.99 (81.76)	–	–	–	–
Smithsonite	3	50.12–54.30 (52.34)	250–420 (350)	0.20–0.25 (0.23)	–	–	–	–	–
Wurtzite	3	65.75–67.34 (66.65)	12,700–13,900 (13,400)	0.04–0.07 (0.05)	–	–	–	–	–

Analyst: Li Sunrong, Institute of Geochemistry, Chinese Academy of Sciences

[a] Single sample

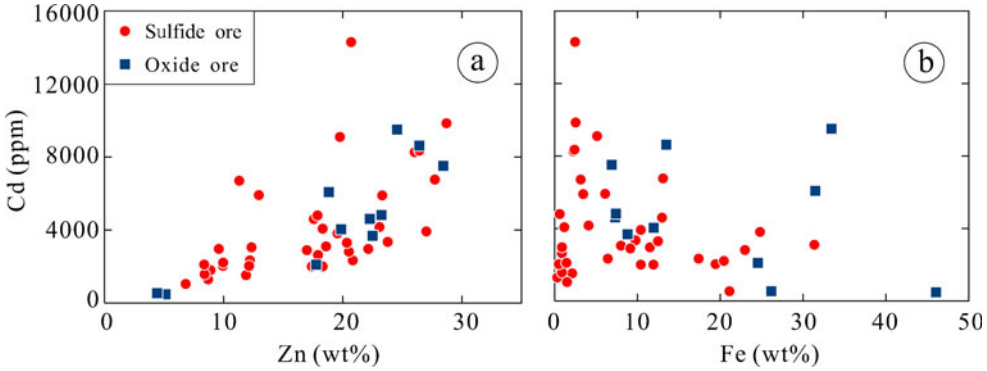

Fig. 3 Binary plots of (**a**) Zn vs. Cd and (**b**) Fe vs. Cd in bulk samples of sulfide and oxide ore, showing inter-element correlations

between Fe and Cd or between S and Cd (Fig. 5) in sphalerite. Moreover, no apparent correlation can be established between Cd and Pb, Fe, or Ag among the sphalerites of different colors. Interestingly, Zn is weakly negatively correlated with Cd with the correlation coefficient of −0.38 (n=19) in light yellow sphalerite. Furthermore, there is a high concentration of Ga in light yellow sphalerite, ranging from 250 to 1,630 ppm (mean 980 ppm, n=9), and one sample shows concentrations of up to 2,900 ppm Ge in light yellow sphalerite. New analytical results by laser ablation inductively coupled mass spectroscopy show that the content of In and Mn is very low in this kind of sphalerite (Ye et al. 2011).

A few wurtzite grains were observed in the ore, coexisting with light yellow sphalerite. These grains are flake-like in shape (1×2 mm), and their identity has been confirmed by X-ray diffraction. Although the content of Cd is relatively high in wurtzite (12,700–13,900 ppm) with an average of 13,400 ppm (n=3), the mineral is not a major Cd carrier in the deposit due to its rarity. In galena, Cd concentrations vary from 830 to 8,685 ppm with an average of 3,233 ppm (n=14), from 183 to 2,500 ppm with an average of 1,345 ppm in pyrite, and from 250 to 420 ppm with an average of 350 ppm in smithsonite (n=3).

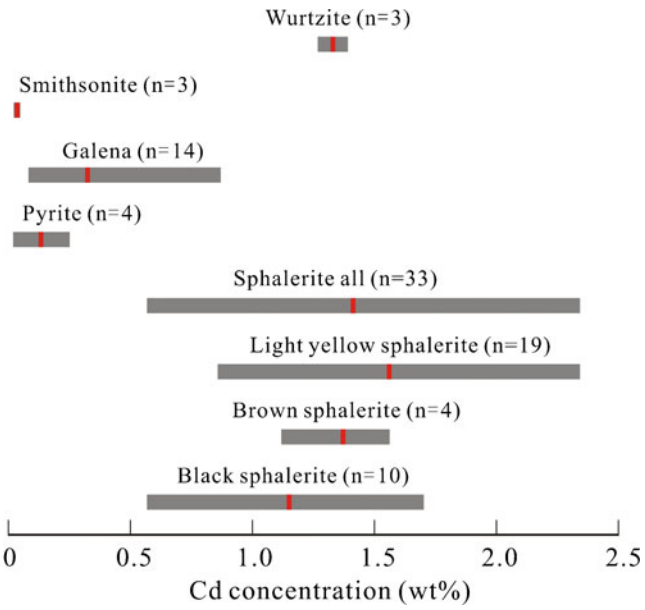

Fig. 4 Schematic diagram depicting the range and mean Cd concentrations in different minerals from the Niujiaotang deposit. Number of analyses are given in *brackets*

Mineralogical siting of cadmium

Cd is similar to Zn both in covalent radius and atomic/ionic structure. The two elements therefore display similar geochemical behaviors. Cd is present isomorphously in sphalerite, but under supergene conditions, Cd may readily be separated from Zn (Liu et al. 1984). Electron microprobe data reveal that the component elements (Zn, S, Cd) are distributed uniformly throughout sphalerite (Appendix B), and no micro-inclusions of Cd-dominant minerals were observed in our scanning electron microscope studies, indicating that Cd is homogeneously distributed as an isomorphous impurity in sphalerite.

Our data show that, in Niujiaotang, Cd occurs dominantly in two forms. Firstly, Cd is present as an isomorphous impurity in sphalerite and subordinately in wurtzite, pyrite, galena, and smithsonite. Secondly, Cd is present as independent minerals. It occurs, for example, as tiny greenockite crystals (~5 μm in size) around the margins of sphalerite grains (Appendix C-a), characteristically in the vicinity of galena inclusions in sphalerite (Appendix C-b); within fractures in irregularly granular, dendritic, and vermiform pyrite (Appendix C-c); and as fine veinlets of greenockite within sphalerite (Appendix C-d). Cadmium also occurs as otavite on the surface of smithsonite grains (Appendix C-e), as greenockite and oxides of Cd or otavite included in smithsonite in the oxidation zone of the deposit (Appendix C-f), and as some orange-colored earthy materials (probably oxides of Cd and greenockite) and encrustations on the surface of Zn oxide ores. Viewed from these modes of occurrence of Cd, primary greenockite may exist in the deposit, although further study would be needed to confirm this. Most of the independent Cd minerals, which occur mostly in the oxidation zone, seem to be clearly secondary. For example, Cd, which is oxidized form

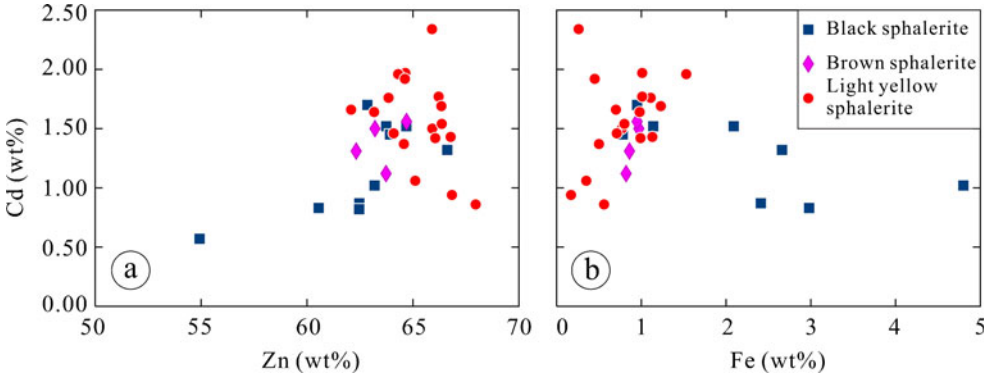

Fig. 5 Binary plots of **a** Zn vs. Cd and **b** Fe vs. Cd in sphalerite of different sub-types

sphalerite, can from $CdSO_4$ replacing sphalerite and subsequently forming greenockite (reaction 1). Cadmium oxides can be transformed into otavite under the action of CO_2 (reaction 2).

$$CdSO_4 + ZnS \rightarrow CdS + ZnSO_4 \quad (1)$$

$$CdO + CO_2 \rightarrow CdCO_3 \quad (2)$$

Fluid inclusion geochemistry

Methodology

All samples were collected from the Mapo II and III ore blocks. The homogenization temperature and ice freezing point of fluid inclusions in sphalerite and calcite were analyzed using a Linkam THMSG600 freezing and heating stage at the State Key Laboratory for Research of Mineral Deposits, Nanjing University. The precision of the determinations is ±0.1°C at temperatures <30°C and ±1°C at >30°C. Bulk fluid inclusion compositions were sampled at 300°C using the decrepitation method and were analyzed by ion chromatography (Shimadzu HIC-SP Super) and gas chromatography (GC2010) at China University of Geosciences, Beijing.

Fluid inclusion geochemistry

Detailed field and microscopic examinations indicate that the mineralization can be divided into three stages (I–III): (1) early mineralization stage, represented by pyrite and black–brown sphalerite; (2) main mineralization stage, represented by light yellow sphalerite; and (3) later mineralization stage (dominantly calcite).

There are few isolated fluid inclusions in stage I brown sphalerite. These are ellipsoid or xenomorphic in shape, between 1.5 and 6 μm in size, and are dominantly liquid-rich inclusions with relatively low vapor/liquid volume ratios (5% to 30%). Fluid inclusions are more abundant in the light yellow sphalerite of stage II. These are also ellipsoid or xenomorphic in shape, range in size between 1 and 12 μm, and have vapor/liquid ratios from 5% to 15%. There are few isolated fluid inclusions in stage III calcite. These are xenomorphic in shape, between 1 and 5 μm in size, and are liquid dominant (vapor/liquid volume ratios from 5% to 10%). In addition, some organic inclusions were observed in light yellow sphalerite and calcite. These are ellipsoid in shape and dark brown in color. Because of their small size (<5 μm), it proved difficult to accurately identify the species present.

The result of homogenization temperature and freezing point measurements for fluid inclusions in sphalerite and calcite are summarized in Table 2; full data are given in Electronic Appendix D. The data show that (a) the temperature of the ore fluid decreased gradually from stage I to III and (b) the salinity and density (calculated by FLINCOR software, Version 1.4; Brown and Lamb 1989) of the ore fluid is higher relatively in stage II. Homogenization temperature data (Fig. 6) show that the temperature of the ore fluid was between 101°C and 142°C (average 120°C), that salinity was between 9.2 and 15.9 wt.% NaCl equiv. (average 13.2 wt.%), and the fluid density was between 1.00 and 1.06 g/cm^3 (average 1.04 g/cm^3) in stage II. These parameters are slightly lower than those of fluid inclusions in MVT deposits (salinity 9~27 wt.% NaCl equiv., density ~1.1 g/cm^3; Roedder 1984; Leach et al. 2005).

As the main mineral in the three mineralization stages, the fluid inclusion compositions of black–brown sphalerite, light yellow sphalerite and calcite were analyzed. Results (Table 3 and Electronic Appendix E) show that in stage I, gas compositions are dominantly H_2O (77.82~95.90 mol%, mean 89.00 mol%, n=3), with subordinate CO_2 (3.08~21.04 mol%, mean 9.94 mol%), CH_4 (0.70~0.91 mol%, mean 0.78 mol%), and N_2 (0.15~0.21 mol%, mean 0.17 mol%, n=3). In stage II, H_2O (70.97~97.26 mol%, mean 88.36 mol%, n=7) and CO_2 (1.14~27.42 mol%, mean 7.94 mol%) are somewhat lower than in the early stage, but N_2 (0.24~6.23 mol%, mean 2.26 mol%, n=7) and CH_4 (0.34~1.44 mol%, mean 0.72 mol%) are significantly higher. Furthermore, C_2H_6 is

Table 2 Summary of homogenization and freezing temperatures, salinity, and density of fluid inclusions

Mineralization stage		Mineral	Homogenization temperature (°C)	Ice-melting temperature (°C)	Salinity (wt.% NaCl equiv.)	Fluid density (g/cm^3)	Number of measurements
Early stage (I)	Mean	Black–brown sphalerite	143.3	−9.7	13.5	1.02	11
	SD		19.8	1.9	2.1	0.02	
	Min		116.8	−12.7	9.1	1.00	
	Max		175.4	−5.9	16.6	1.04	
Main stage (II)	Mean	Light yellow sphalerite	120.3	−9.4	13.2	1.04	15
	SD		12.3	1.9	2.2	0.02	
	Min		101.4	−11.9	9.2	1.00	
	Max		142.5	−6.0	15.9	1.06	
Late stage (III)	Mean	Calcite	112.2	−2.9	4.6	0.98	12
	SD		12.4	0.8	1.2	0.01	
	Min		90.4	−3.7	2.5	0.97	
	Max		128.4	−1.5	5.9	0.99	

also identified (0~0.56 mol%, mean 0.47 mol%), implying involvement of organic material in the mineralizing event. In the late mineralization stage, H_2O (75.27~97.13 mol%, mean 91.87 mol%, n=8) and CO_2 (1.98~23.39 mol%, mean 6.06 mol%) are the lowest. Other than these, there are no other obvious compositional changes from main to late stages of mineralization.

Cation components are dominated by Ca^{2+}, Mg^{2+}, Na^+, and K^+, and the main anions present in the main mineralization stage are SO_4^{2-}, Cl^-, and F^- (Table 3; Electronic Appendix E). The order of ionic percentage composition is $Ca^{2+}>Mg^{2+}>Na^+>K^+$, which is similar to that of fluid inclusions in MVT deposits (Roedder 1984), except that Ca^{2+} and Mg^{2+} contents are relatively higher. From stages I to III, the SO_4^{2-} content gradually decreases, F^- displays no obvious change, and Cl^- is relatively higher in inclusions from stage II. Moreover, the ore-forming fluid is rich in Na^+ and poor in K^+ with Na^+/K^+ ratio between 0.78 and 4.00 (mostly >1.00), and the $Na^+/(Ca^{2+}+Mg^{2+})$ ratio is <1. According to Roedder (1972), the Na^+/K^+ ratio of magmatic hydrothermal inclusions is usually <1, and the mineralization fluid of typical hot brine is characterized by higher Na^+/K^+ ratio with $Na^+/(Ca^{2+}+Mg^{2+})$ ratio >1.

Isotope geochemistry

Methodology

Three sulfides (sphalerite, pyrite, and galena) were separated by hand and checked for purity (which exceeded 99%). After washing with 0.15 mol/L HCl and Milli-Q water (for sulfides) or Milli-Q® water (for carbonates), sulfide samples were crushed and sieved, then ground to <200 mesh

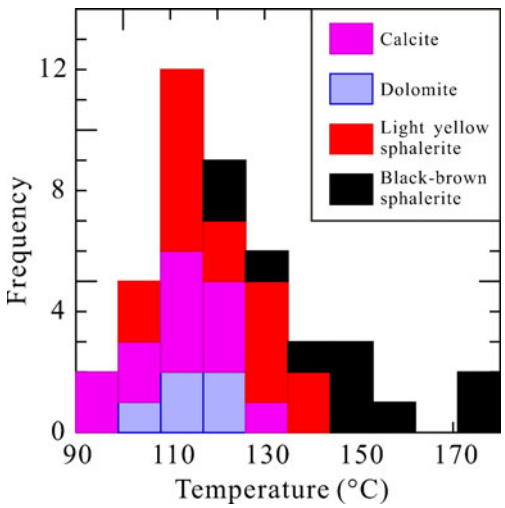

Fig. 6 Histogram showing distribution of fluid inclusion homogenization temperatures

Table 3 Composition of inclusions in Niujiaotang deposit and the physicochemical parameters

	Mineralization stage	Early stage (I)				Main stage (II)				Later stage(III)			
	Mineral	Black–brown sphalerite				Light yellow sphalerite				Calcite			
		Mean	Min	Max	SD	Mean	Min	Max	SD	Mean	Min	Max	SD
Cation components (μg/g)	K^+	6.36	4.88	7.53	1.35	11.72	7.67	23.44	7.82	6.88	2.69	14.63	4.51
	Na^+	9.48	5.20	12.13	3.74	12.86	6.08	25.70	8.77	14.76	3.99	41.64	11.90
	Ca^{2+}	73.42	50.99	89.12	19.94	50.04	27.62	72.05	22.22	179.49	71.23	384.85	107.53
	Mg^{2+}	38.08	10.03	55.23	24.49	24.47	13.80	41.77	15.12	61.60	26.61	180.04	50.49
	F^-	2.53	1.11	3.77	1.34	2.68	1.66	4.02	1.03	4.79	2.06	18.00	5.44
	Cl^-	17.96	10.39	22.59	6.61	21.80	5.52	42.80	15.49	19.35	4.99	100.51	32.90
	SO_4^{2-}	1,115.8	578.8	1,432.1	467.5	491.8	260.2	667.2	169.4	127.4	12.7	851.8	292.8
Gas compositions (mol%)	H_2	0.10	0.05	0.16	0.06	0.25	0.17	0.34	0.06	0.42	0.22	0.84	0.24
	N_2	0.17	0.15	0.21	0.03	2.26	0.24	6.23	2.81	1.42	0.35	3.23	1.00
	CH_4	0.78	0.70	0.91	0.11	0.72	0.34	1.44	0.45	0.22	0.17	0.36	0.06
	C_2H_6	<mdl	<mdl	<mdl		0.47	<mdl	0.56	0.07	<mdl	<mdl	<mdl	
	CO_2	9.94	3.08	21.04	9.92	7.94	1.14	27.42	9.41	6.06	1.98	23.39	6.98
	H_2O	89.00	77.82	95.90	9.99	88.36	70.97	97.26	9.18	91.87	75.27	97.13	6.69
Na^+/K^+	1.56	0.78	2.28	0.75	1.09	0.79	1.33	0.23	2.30	1.00	4.00	1.20	
Na/(Ca+Mg)	0.10	0.04	0.18	0.07	0.13	0.08	0.16	0.04	0.07	0.02	0.21	0.06	
F^-/Cl^-	0.14	0.11	0.17	0.03	0.17	0.07	0.30	0.10	0.37	0.18	0.54	0.14	
CO_2/H_2O	0.11	0.03	0.27	0.13	0.09	0.01	0.39	0.13	0.07	0.02	0.31	0.10	
CO_2/CH_4	12.67	4.19	23.04	10.21	10.98	1.57	80.23	28.73	27.08	10.68	101.42	29.85	
$(CH_4+CO)/CO_2$	0.08	0.04	0.24	0.10	0.09	0.01	0.64	0.26	0.04	0.01	0.09	0.03	
$(H_2+CH_4+CO)/CO_2$	0.09	0.05	0.26	0.11	0.12	0.02	0.74	0.31	0.11	0.04	0.27	0.08	

NO_3^-, O_2, and CO below detection limit in all analyses

(75 μm). After removal of the adsorbents on the sample surface, the whole rock and ore samples were ground as fine as <200 mesh. Sulfur isotope determinations of sulfides were made at the Isotope Analysis Center, Yichang Institute of Geology and Mineral Resources, Chinese Academy of Geological Sciences (YIGMR-CAS). The crushed samples were then mixed with CuO in varying proportions (sphalerite/CuO=1 6, galena/CuO=1 4, and pyrite/CuO=1 6) and heated at 1,050–1,060°C for 15 min in a muffle furnace in order to produce SO_2. The sulfur isotopic composition of SO_2 gas was measured on a Finnigan MAT-251 mass spectrometer, using the LTB-2 standard ($\delta^{34}S_{CDT}$=1.84±0.2‰). The precision of the method is about 0.2‰.

For analysis of Pb isotopes, the sulfide mineral powder was digested in aqua regia and carbonate samples by HCl in Sevillex vials. The solution was heated until incipient dryness and was then converted to a 1.5-mol/L HCl+ 0.65 mol/L HBr solution. Lead was separated by chromatography on Bio-Rad AG-1×8 anion exchange resin and then eluted using 1.0 mol/L HNO_3. For sphalerite, a large amount of 0.15 mol/L HBr was eluted until Zn was entirely removed before Pb was eluted using 1.0 mol/L HNO_3. The solution was evaporated to dryness, and Pb was ready for mass spectrometry. All acids used were double-distilled in a two-bottle distiller. Lead was loaded onto a Re ribbon using silica gel and Pb isotopic ratios analyzed on a Finnigan MAT-262 multi-collector thermal ionization mass spectrometer by static mode at the Isotope Analysis Center of YIGMR-CAS. Measured isotopic ratios were corrected for a mass fractionation of 0.096% per atomic mass unit determined by replicate measurements of reference sample SRM 981.

Results—sulfur isotopes

The ore minerals are mainly sphalerite, pyrite, and galena, and no sulfates are observed in the deposit. Published sulfur isotope data for the three sulfides are presented in Electronic Appendix F and Fig. 7. The deposit is ^{34}S-rich and thus analogous to MVT Pb–Zn deposits ($\delta^{34}S$=+10~+25‰; Leach and Sangster 1993). $\delta^{34}S$ values for sulfides show a roughly normal distribution and range from +10.0‰ to +32.8‰ (total range 22.7‰, mean value +22.5‰). $\delta^{34}S$ values vary from +10.0‰ to +29.8‰ for sphalerite (mean +25.2‰, n=24), from +22.6‰ to +29.0‰ for pyrite (mean +25.7‰, n=8), and from +20.3‰ to +32.8‰ for galena (mean +26.0‰, n=6). $\delta^{34}S$ values follow the order $\delta^{34}S_{pyrite}>\delta^{34}S_{sphalerite}>\delta^{34}S_{galena}$ when the minerals coexist, implying that sulfur isotope distributions are in equilibrium.

The $\delta^{34}S$ values of sulfides can represent the total sulfur isotopic compositions of the ore-forming fluid (Ohmoto 1972), i.e., $\delta^{34}S\Sigma S\approx\delta^{34}S$ sulfide. The sulfur isotopic

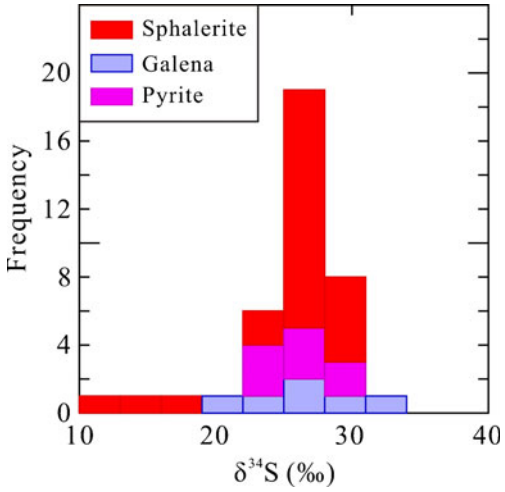

Fig. 7 Histogram showing distribution of $\delta^{34}S$ in sulfides

compositions of ore sulfides may thus be used to trace the source of sulfur in the ore-forming fluids. The sulfur isotope signature of the deposit indicates that sulfur may have been derived from two distinct sources: (1) sulfate sulfur in Cambrian strata or strata-confined water and (2) oil-field brine. Although the S-isotope signature of the deposit closely resembles that of Cambrian seawater ($\delta^{34}S$=+15~+35‰; Claypool et al. 1980), there are strong arguments favoring an oil-field brine fluid. The Niujiaotang deposit is located in the southern part of the Majiang paleoreservoir, and dry bitumen is abundant in the ore district; its S-isotope composition lies between +22.6‰ and +26.2‰ (Wang and Shi 1997), similar to the sulfides in the Niujiaotang deposit. Apart from this, bitumen and gaseous hydrocarbon are abundant in ore-forming fluid inclusions and in oil and gas reservoir trap structures elsewhere in the Xiangxi–Qiandong Pb–Zn metallogenic belt (Pu et al. 1993) strongly suggesting that part of the ore sulfur was derived from oil-field brines.

Using the isotope fractionation equation of Ohmoto and Rye (1979) for the mineral pair sphalerite–galena in samples where $\delta^{34}S_{pyrite}>\delta^{34}S_{sphalerite}>\delta^{34}S_{galena}$, mineralization temperatures of between 102±10°C and 121±10°C are derived for the Niujiaotang deposit. Such values correspond well with the homogenization temperatures of fluid inclusions (see above).

Results—lead isotopes

Lead isotopic compositions of sphalerite, galena, ores, and host rocks from Niujiaotang deposit are summarized in Table 4 (full data in Electronic Appendix G) and shown graphically in Fig. 8. The characteristics can be described as follows:

Table 4 Summary of Pb isotopic composition of sulfides, ores, and host lithologies in the Niujiaotang deposit

Name of sample	Number of samples	Analytical results (mean given in brackets)			Model age (Ma)	μ value
		Range of isotopic ratio				
		$^{206}Pb/^{204}Pb$	$^{207}Pb/^{204}Pb$	$^{208}Pb/^{204}Pb$		
Qingxudong formation dolostone	2	17.204–17.584 (17.394)	15.479–15.491 (15.485)	38.138–38.333 (38.236)	633–888 (761)	9.35–9.40 (9.38)
Wuxun formation shale with thin limestone	2	18.559–19.073 (18.816)	15.646–15.723 (15.685)	38.956–39.408 (39.182)	116–161	9.54–9.64 (9.59)
Sphalerite	5	18.057–18.226 (18.140)	15.621–15.754 (15.680)	38.099–38.463 (38.252)	433–510 (461)	9.54–9.79 (9.65)
Galena	3	18.196–18.203 (18.200)	15.724–15.736 (15.732)	38.346–38.401 (38.382)	467–478 (474)	9.74–9.76 (9.75)
Whole ore (Zn–Pb)	7	18.148–18.266 (18.204)	15.674–15.802 (15.734)	38.214–38.651 (38.391)	443–506 (471)	9.64–9.88 (9.75)

1. Different sulfide minerals and ores have homogeneous and characteristically low radiogenic Pb isotopic compositions with higher μ values (9.54~9.88), Th/U ratio, and narrow ranges of variation (<0.1% relative). The ratios $^{206}Pb/^{204}Pb$, $^{207}Pb/^{204}Pb$, and $^{208}Pb/^{204}Pb$ for sphalerite range from 18.057 to 18.226, 15.724 to 15.736, and 38.099 to 38.463, respectively; those for galena range from 18.196 to 18.203, 15.621 to 15.754, and 38.346 to 38.401, respectively; and those for the bulk ore, from 18.148 to 18.266, 15.674 to 15.802, and 38.214 to 38.651, respectively. The μ value varies from 9.54 to 9.79 for sphalerite, 9.74 to 9.76 for galena, and 9.74 to 9.76 for bulk ore. Sphalerite and galena model ages of 433~510 Ma are obtained. These are comparable with the age of the host strata, suggesting that the deposit is coeval with, or slightly later than the host strata.
2. The Pb isotope compositions of the host lithologies are little different to those of the ores and sulfide separates. $^{206}Pb/^{204}Pb$, $^{207}Pb/^{204}Pb$, and $^{208}Pb/^{204}Pb$ ratios for the Qingxudong Formation dolomite range from 17.204 to 17.584, 15.479 to 15.491, and 18.559 to 19.073, respectively, with μ=9.35~9.40; ratios for Wuxun Formation shale with thin limestone range from 18.559~19.073, 15.646 to 15.723, and 38.956 to 39.408, respectively, with μ=9.54 to 9.64. The data show that the Pb isotope compositions of different sulfides and ores are both consistent and also similar to those of the Wuxun Formation shale with thin limestone (ϵ_w). They are distinct from the signatures of the Qingxudong Formation (ϵ_q) algae-bearing dolostones.
3. Compared with the Pb isotopic model of Zartman and Doe (1981), most samples lie above the upper crustal Pb curve (Fig. 8a) or adjacent to the orogenic Pb curve (Fig. 8b). They are characteristic of upper crustal lead, suggesting that the ore lead of the deposits was probably derived from upper crustal rocks which are relatively rich in U and Th.

Discussion

Source of ore-forming metals and sulfur

Previous research (Wang and Shi 1997; Chen et al. 2005) shows that the background value of ore-forming elements (e.g., Zn, Pb, As, Sb, etc.) in the Cambrian host rocks is several times higher than in other strata in the region. The Early Cambrian Wuxun Formation is particularly enriched in Zn (mean 98.6 ppm) and Pb (mean 23.6 ppm). Our analytical results show that Cd concentrations are 10~20 ppm in regional dolostones (Early Cambrian Qingxudong Formation) and up to 40~340 ppm in the dolostone wallrocks hosting the

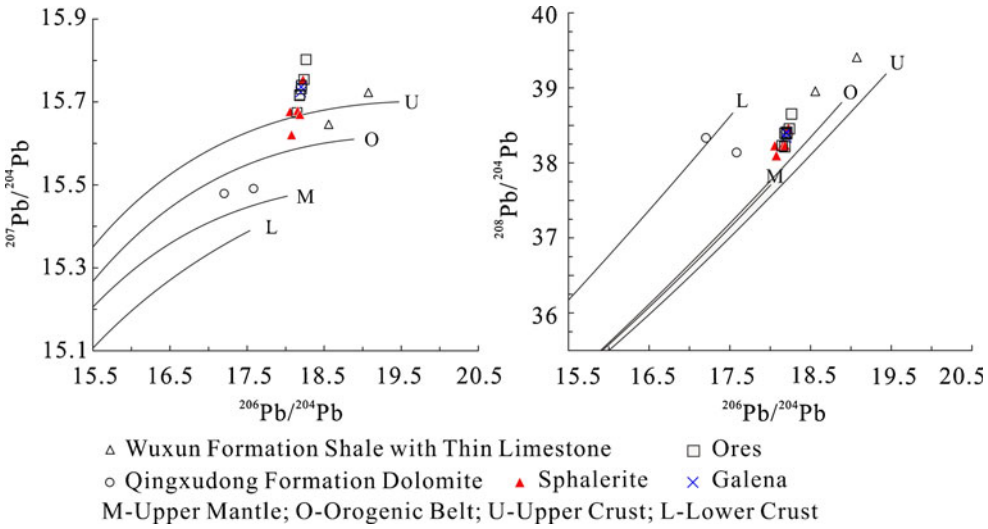

Fig. 8 Plots of **a** $^{206}Pb/^{204}Pb$ vs. $^{207}Pb/^{204}Pb$ and **b** $^{206}Pb/^{204}Pb$ vs. $^{208}Pb/^{204}$ Pb (after Zartman and Doe 1981) for whole rocks and sulfide separates from the Niujiaotang deposit

ore (Table 1), i.e., several orders of magnitude higher than the crustal abundance of Cd (about 0.08 ppm; Rudnick and Gao 2005). The area is thus clearly highly anomalous with respect to high background Cd and could have supplied significant quantities of Cd to form an ore deposit. Furthermore, the Pb isotope compositions of different sulfides and ores are characteristic of upper crustal lead and closely resemble those of the Early Cambrian Wuxun Formation strata, implying that the latter is likely to have been an important source of ore-forming material.

The Niujiaotang deposit is characterized by a heavy sulfur isotope signature. The sulfur isotope composition of sulfides is similar to that of sulfate sulfur in Cambrian strata and that of oil-field brines (bitumen). A few sulfate minerals (e.g., gypsum) were, however, found in wallrock over- and underlying the ore, leading us to suggest that the Cambrian strata could have supplied sufficient reduced sulfur during the mineralization process. Normally, there is a close relationship between the sulfur isotope composition of oil-field brines (bitumen) and that of contemporaneous sulfate deposited on the seafloor (Faure 1986); hence, the sulfur isotopic composition of dry bitumen in the Majiang paleoreservoir is also rich in heavy sulfur isotopes, similar to that of sulfate sulfur in Cambrian strata. It is suggested that the oil-field brine may be the potential source of sulfur for the deposit. The high background sulfur in the combustible fraction of bitumen from the main paleo-oil reservoirs in Guizhou Province (0.3~8 wt.%, mean 3.0 wt.%, n=12; Wang and Shi 1997) also supports this argument.

Source of ore-forming fluid

The results of fluid inclusion analysis show that the ore fluid is a low-temperature Na^{+}–Ca^{2+}–Mg^{2+}–Cl^{-} system, which can be considered as broadly similar to what has been identified in MVT deposits, but nevertheless slightly different with respect to temperature, salinity, and density of the ore fluid (Fig. 9). Except for the higher Ca^{2+} and Mg^{2+} contents, which may be related to the later carbonation stage, the composition of the ore fluid is similar to oil-field brine. Increasing amounts of data indicate that there are close relationships between low-temperature Pb–Zn deposits and nearby petroleum paleoreservoirs (e.g., Li 1999). For example, the mineralizing fluid of the Laisvall Pb–Zn deposit, Sweden, is rich in hydrocarbons (Rickard et al. 1975). Moreover, the metallogenic model for the Huayuan Pb–Zn deposit, Hunan province, China, located in the same Pb–Zn metallogenic belt as Niujiaotang, involves destruction of a petroleum paleoreservoir (Ye et al. 1998). It is thus suggested that the mineralizing fluid involved in formation of the Niujiaotang deposit may have some relationship with oil-field brines of the Majiang petroleum paleoreservoir (Figs. 9 and 10).

The following evidence also supports such a hypothesis: (1) Black bitumen is found in nearby orebodies and is abundant in many other deposits in the Xiangxi–Qiandong Pb–Zn belt, such as Huayuan, Xiunao, Maopo, Zhuping, Yongxi, Wengxi, Yebadong, Longjingjie, Bosong, Duniu, etc. (Wang 1993, 1996; Zhang et al. 1994; Wang and Shi 1997; Chen et al. 1992, 2005); (2) the concentration of Zn in bitumen is between 3.8 and 73 ppm with an average of 22.6 ppm in Majiang region (Hu et al. 2007); (3) organic inclusions occur in the light yellow sphalerite and calcite; (4) CH_4 and C_2H_6 increase significantly in the main mineralization stage; and (5) Wang (1993, 1996) used Pb isotopes to give an Ordovician galena model age for the deposit. This age (475~499 Ma) is in accord with that of other Pb–Zn deposits in Xiangxi–Qiandong Pb–Zn zone (Wang 1993; Zhang et al. 1994). The Majiang paleoreservoir formed during the Early Cambrian and was destroyed during the Ordovician (Zhang 1987a; Xiang et al. 2008) corresponding with the timing of ore formation at Niujiaotang.

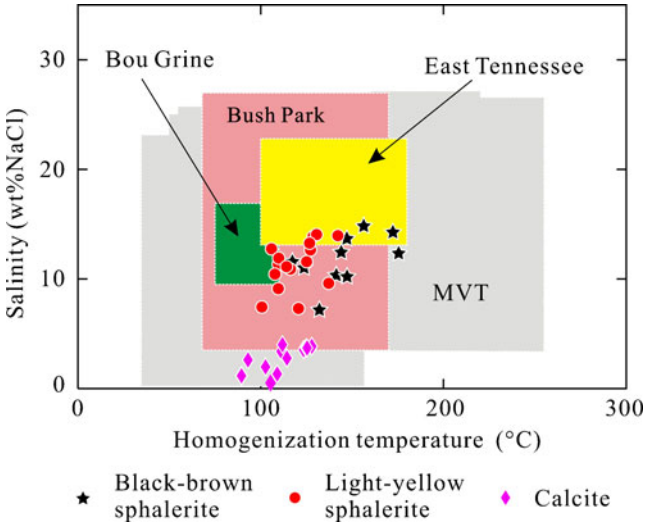

Fig. 9 Diagram of fluid inclusion homogenization temperature and salinity values for the Niujiaotang deposit compared with data for MVT deposits worldwide (data from Leach et al. 2005)

There are many arguments favoring a genetic relationship between oil-field brines and the formation of MVT Pb–Zn deposits (e.g., Leach et al. 2005). High metal concentrations are found in most oil-field brines (Carpenter et al. 1974; Kharaka et al. 1987; Saunders and Swann 1990; Emsbo 2000). Pb and Zn concentrations are up to several hundred parts per million and correlate negatively with the content of reducing sulfur. Moreover, the pH of oil-field brines is mostly around 5 to 6, closely resembling that of ore-forming fluids in MVT systems (Emsbo 2000). Oil-field brines may thus be a effective carrier of metals such as Pb and Zn and, under the right conditions, could transport the metals over significant distances within sedimentary sequences (Giordano and Barnes 1981; Sverjensky 1984; Hennet et al. 1988; Surdam et al. 1989; Disnar 1990; Vlassopoulos et al. 1990). Oil-field waters of $CaCl_2$ type

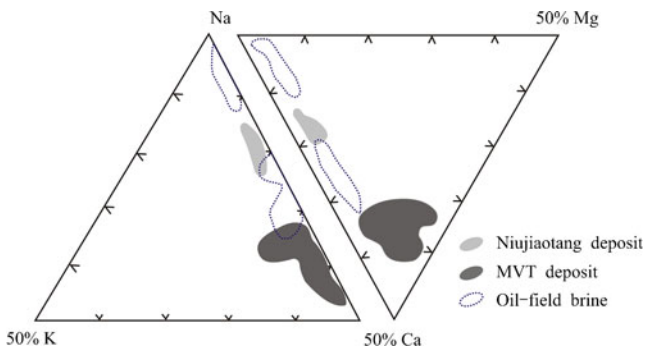

Fig. 10 Atomic ratios of Na, K, Ca, and Mg in Niujiaotang ore-forming fluids (after Rui et al. 1991). Compositions of Mississippi Valley-type fluids (Hall and Friedman 1963; Roedder et al. 1963) and oil-field brines (Graf et al. 1966; Carpenter et al. 1974) are shown for comparison

are most efficient for dissolution and transportation of Pb and Zn (e.g., Carothers and Kharaka 1978; Kharaka et al. 1986; Cao et al. 2002).

The ore-forming fluid of Niujiaotang is considered to be an oil-field brine which evolved from the destruction of the Majiang petroleum paleoreservoir. The Majiang petroleum paleoreservoir was uplifted and destroyed during the Ordovician Guangxi tectonic movement, leading to escape of liquid hydrocarbons and migration of oil-field brine from the center of the basin to the margin. In the Niujiaotang area, Zn and Cd, particularly in the Qingxudong and Wuxun Formations, were mobilized by hot oil-field brines rising along the Zaolou fault system and formed stratiform and generally conformable Zn–Cd orebodies in reactive carbonate lithologies. Calcite and dolomite were also formed in the orefield as a result of this interaction. Calculations from our fluid inclusion data (Table 3) show that the CO_2/CH_4 ratio (1.57~80.23) is the lowest and the $(H_2+CH_4+CO)/CO_2$ ratio (0.02~0.74) is the highest in ore fluid of main mineralizing stage, implying that the ore fluid was weakly reducing. Furthermore, the ore fluid, which contains high SO_4^{2-} and Cl^-, with $Cl^->F^-$ and $Na^+>K^+$, has the composition of an evolved oil-field brine. It is suggested that the metals were transported as HS^-, Cl^-, and organic complexes.

Deposit type

No igneous rocks are recognized anywhere in the region, implying that the formation of the Niujiaotang deposit is unrelated to magmatic activity. The orebody is hosted in algae-bearing dolostones of the Early Cambrian Qingxudong Formation. Ores are stratabound and occur as beds or lenticular bodies.

The oolitic, framboidal, bioclastic, and microbedding textures of pyrite with minor sphalerite are syngenetic in origin. It is commonly observed, in nearby orebodies, that the dolomite is recrystallized and sedimentary textures are overprinted although a few are preserved. The ores display metasomatic relict textures, metasomatic resorption, and vein textures, all demonstrating the multiphase character of the mineralization. In addition, all deposits in the area (e.g., Niujiaotang, Duniu, Dongchong Pb–Zn deposit) are controlled by the Mandong fault and occur within a 2–3-km range of the northwestern side of the fault, also strongly suggesting that the mineralization at Niujiaotang relates to, or at least was strongly influenced by, tectonic deformation and concomitant fluid movement (Zhang et al. 1994; Fig. 1).

Based on Zhang Qian's studies of trace elements in sphalerite from 36 major typical Pb–Zn deposits throughout the world (Zhang 1987b), sphalerite of different origin can be readily distinguished on Cd vs. Fe diagrams. As seen in Fig. 11, sphalerite from the Niujiaotang deposit plots within

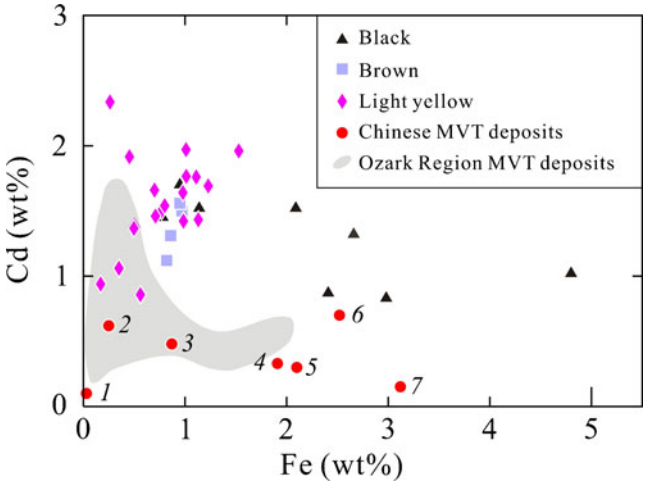

Fig. 11 Plot of Fe vs. Cd for differently colored sphalerite from the Niujiaotang deposit, compared to a number of Chinese MVT deposits (after Zhang 1987b) and for MVT deposits in the Ozark Region, USA (Viets et al. 1992). Key to Chinese MVT deposits: *1* Shashulin, *2* Yutang, *3* Chahe, *4* Tianbaoshan, *5* Qixiashan, *6* Daliangzi, *7* Fankou

the field of low-temperature hydrothermal deposits, such as MVT deposits, but its Cd content is higher than that of MVT deposits in the Ozark Region, USA (Viets et al. 1992) and especially higher than that of many Chinese MVT deposits (Fankou, Daliangzi, Tianbaoshan, Shashulin, Yutang, Chahe, Qixiashan, etc.).

It is generally believed (e.g., Liu et al. 1984) that light-colored sphalerite forms at lower temperatures and typically contains higher contents of Cd, Ge, and Ga but is relatively poor in Fe and In. Sphalerite from the Niujiaotang deposit is mainly bright yellow in color and is high in Cd (0.83~1.54 wt.%, mostly >1.10 wt.%, with a maximum of 1.97 wt.%), obviously higher than in other Pb–Zn deposits such as Jinding, Fankou, and Dongshengmiao. The sphalerite is also rich in Ga, but relatively poor in Ag, Fe, Mn, and In. As shown in Table 5, these chemical characteristics are similar to sphalerite in MVT Pb–Zn deposits but distinct from those from high-temperature hydrothermal Pb–Zn ores.

Conclusions

1. The Niujiaotang deposit is a MVT deposit. Sphalerite in the deposit is abnormally Cd rich, representing a resource in excess of 5,000 tonnes Cd metal (and thus a large deposit of this element in the Chinese classification system). Ga and Ge are also found in relatively high concentrations and are of potential economic interest as by-products.
2. Cadmium mostly occurs as an isomorphous impurity in sphalerite. Independent minerals of cadmium (e.g., greenockite and otavite), which occur mostly in the oxidation zone of the deposit, are present in small

Table 5 Comparison of sphalerite compositions among Pb–Zn deposits of different types (parts per million)

Deposit type	MVT deposits			High-temperature hydrothermal deposits				
	Niujiaotang	Fankou	Upper Mississippi	Xiaotieshan	Xietieshan	Caijiaying	Yinshan	Shuikoushan
Fe (wt.%)	0.80–4.80	5.01	1.41	4.11	11.68	5.96	4.20	3.81
Zn (wt.%)	60.55–65.11	59.90	65.09	64.63	55.37		62.94	56.30
Cd (wt.%)	0.83–1.97	0.19	0.23	0.31	0.20	0.29	0.22	0.25
Ag	1.40–73.45	195	21	202	18	27	1,112	118
Ga	230–1,630	345	95	20	9	2	50	55
Ge	2,900	95	102	<1	0.2	7	4	3
In	Trace	7	Trace	38	431	68	142	47
Mn	Trace	125	49			1,750	688	2,770
Zn/Cd	31.27–75.25	324	283	208	277		287	225
Cd concentration coefficient	30.47–72.96	7.04	8.52	11.52	7.41	10.74	8.15	9.26

The data for Niujiaotang are from this paper, those of Caijiaying are from Pan et al. (1993); all others are from Rui et al. (1991)
Cd concentration coefficient = sample content/240 ppm (minimum mining grade)

amounts in the primary ore but are probably secondary minerals formed during weathering–leaching processes.

3. Geochemical data indicate that the metals in the Niujiaotang deposit such as Cd and Zn are mainly derived from the Early Cambrian Qingxudong and Wuxun Formations. Sulfur came from oil-field brines of the Majiang paleoreservoir, and the mineralizing fluid is likely to have been a migrating oil-field brine.
4. An improved metallogenic model for the deposit can be given: During the Early Cambrian, the Niujiaotang area was a shallow-sea environment marginal to a platform (Chen et al. 1992). Zinc and Cd in seawater were concentrated in abundant algae, via as-yet unconstrained biological mechanisms, resulting in large amounts of algal ooliths which were rich in Zn and Cd. In the Ordovician, accompanying the destruction of the Majiang petroleum paleoreservoir (Zhang 1987a), an oil-field brine migrated to the basin margin. In the Niujiaotang ore district, Zn and Cd in the Cambrian strata, particularly in the Qingxudong and Wuxun Formations, were mobilized by the brines that rose along the Zaolou fault system. Stratiform Cd-rich zinc orebodies were formed that are conformable with the host lithologies.

Acknowledgments This work was jointly funded by the National Natural Science Foundation of China (Grant No. 40373021) and the State Key Laboratory of Ore Deposit Geochemistry, Institute of Geochemistry, Chinese Academy of Sciences. We thank the *Mineralium Deposita* reviewers for their constructive comments on this manuscript and Editor-in-Chief Bernd Lehmann for his helpful suggestions. This manuscript was prepared during the senior author's sabbatical visit in Adelaide funded by the Chinese National Science Foundation. This is TRaX contribution no. 139.

References

Balabin AI, Urusov VS (1995) Recalibration of the sphalerite cosmobarometer: experimental and theoretical treatment. Geochim Cosmochim Acta 59:1401–1410

Barton PB Jr, Behre CH Jr (1954) Interpretation and evaluation of the uranium occurrences near Goodspring, Nevada. US Atomic Energy Comm. RME-3119, pp 1–105

Barton PB, Toulmin P III (1966) Phase relations involving in the Fe–Zn–S system. Econ Geol 61:815–849

Bortnikov NS, Dobrovol'skaya MG, Genkin AD, Naumov VB, Shapenko VV (1995) Sphalerite-galena geothermometer: distribution of cadmium, manganese, and the fractionation of sulfur isotopes. Econ Geol 90:155–180

Brown AC (1974) An epigenetic origin for stratiform Cd–Pb–Zn sulfides in the lower Nonesuch Shale, White Pine, Michigan. Econ Geol 69:271–274

Brown PE, Lamb WM (1989) P–V–T properties of fluids in the system H_2O–CO_2–NaCl: new graphical presentations and implications for fluid inclusion studies. Geochim Cosmochim Acta 53:1209–1221

Cabri LJ, Blank H, El Goresy A, Laflamme JHG, Nobiling R, Sizgoric MB, Traxel K (1984) Quantitative trace element analyses of sulphides from Sudbury and Stillwater by proton microprobe. Can Mineral 22:521–542

Cao H-L, Hua R-M, Rao B, Qiu L-W (2002) Preliminary experimental study on dissolution of metal elements in oil field brine of Jiyang depression, Shandong Province. Geol Rev 48(4):444–448 (in Chinese with English abstract)

Carothers WW, Kharaka YK (1978) Aliphatic acid anions in oil field waters implication for origin of natural gas. AAPG Bull 62:2441–2456

Carpenter AB, Trout M, Pickett EE (1974) Preliminary report on the origin and zinc-rich oil field basin of Central Mississippi. Econ Geol 68:1191–1206

Černý P, Harris DC (1978) The Tanco pegmatite at Bernic Lake, Manitoba. XI. Native elements, alloys, sulfides and sulfosalts. Can Mineral 15:625–640

Chaplygin IV, Mozgova NN, Mokhov AV, Koporulina EV, Bernhardt H-J, Bryzgalov IA (2007) Minerals of the system ZnS–CdS from fumaroles of the Kudriavy Volcano, Iturup Island, Kuriles, Russia. Can Mineral 45:709–722

Chen TT, Dutrizac JE (1978) Lautite and cadmium-rich sphalerite from the Ross Mine, Hislop Township, Ontario. Can Mineral 16:665–669

Chen G-Y, Zhong Y-T, Huang G-S (1992) Geological characters and conditions of mineralization of Niujiaotang zinc deposit. Duyun. Guizhou Geology 9:203–211 (in Chinese)

Chen G-Y, An Q, Fan Y-M (2005) Geologic characteristic of the lead–zinc deposits in the Eastern Guizhou and analysis on metallogenesis. Guizhou Geology 22:252–259 (in Chinese with English abstract)

Claypool GE, Holser WT, Kaplan IR, Sakai H, Zak I (1980) The age curves of sulfur and oxygen isotopes in marine sulfate and their mutual interpretations. Chem Geol 28:199–260

Cook NJ, Ciobanu CL, Pring A, Skinner W, Shimizu M, Danyushevsky L, Saini-Eidukat B (2009) Trace and minor elements in sphalerite: a LA-ICPMS study. Geochim Cosmochim Acta 73:4761–4791

Di Leo PD (2000) A nuclear magnetic resonance (NMR) and Fourier-transform infrared (FTIR) study of glycine speciation on a Cd-rich montmorillonite. Clay Clay Miner 48:495–502

Disnar JR (1990) Organic matter in ore genesis: progress and perspectives. Org Geochem 16:577–599

Dobbe RTM (1992) Manganoan–cadmian tetrahedrite from the Tunaberg Cu–Co deposit, Berglagen, central Sweden. Mineral Mag 56:113–115

Emsbo P (2000) Gold in Sedex deposits. Rev Econ Geol 13:427–437

Faure G (1986) Principles of isotope geology, 2nd edn. Wiley, New York, p 589

Giester G, Rieck B, Brandstätter F (1998) Niedermayrite, $Cu_4Cd(SO_4)_2(OH)_6{\cdot}4H_2O$, a new mineral from the Lavrion mining district, Greece. Mineral Petrol 63:19–34

Giordano TH, Barnes HL (1981) Lead transport in Mississippi Valley-type ore solutions. Econ Geol 76:2200–2211

Gottesmann W, Kampe A (2007) Zn/Cd ratios in calcsilicate-hosted sphalerite ores at Tumurtijn-ovoo, Mongolia. Chemie Erde 67:323–328

Gottesmann W, Gottesmann B, Seifert W (2009) Sphalerite composition and ore genesis at the Tumurtjin-ovoo Fe–Mn–Zn skarn deposit, Mongolia. Neues Jb Mineral Abh 185:249–280

Graf DL, Meents WF, Friedman I, Shimp NF (1966) The origin of saline formation waters, III: Calcium chloride waters. Geol Surv Circ 397:1–60

Hall W, Friedman I (1963) Composition of fluid inclusions, cave-in-rock fluorite district, Illinois, and Upper Mississippi valley zinc–lead district. Econ Geol 58:886–911

Han S-Q, Wang S-D, Hu W-Y (1982) The discovery of a paleopool in Majiang and its geological significance. Oil Gas Geology 3(3–4):316–326 (in Chinese with English abstract)

Hennet RJC, Crerar DA, Schwartz J (1988) Organic complexes in hydrothermal system. Econ Geol 83:742–764

Hitzman MW (2001) Zinc oxide and zinc silicate deposits—a new look. Geol Soc Am Ann Meeting, Abstr Program 33:A336

Hu Y-Z, Han R-S, Mao X-X (2007) Relationship between metal mineralization and accumulation of oil and gas in the Eastern Guizhou. Geology Prospecting 43:51–56 (in Chinese with English abstract)

Järup L, Åkesson A (2009) Current status of cadmium as an environmental health problem. Toxicol Appl Pharmacol 238:201–208

Kelley KD, Leach DL, Johnson CA, Clark JL, Fayek M, Slack JF, Anderson VM, Ayuso LE, Ridley WI (2004) Textural, compositional, and sulfur isotope variations of sulfide minerals in the Red Dog Zn–Pb–Ag deposits, Brooks Range, Alaska: implications for ore formation. Econ Geol 99:1509–1532

Kharaka YK, Law LM, Carothers WW (1986) Role of organic species dissolved in formation water from sedimentary basin in mineral diagenesis. In: Gautier DL (ed) Role of organic matter in sedimentary diagenesis. Soc Econ. Paleontol Mineral Spec Publ 38. Tulsa, Society of Economic Paleontologists and Mineralogists, pp 111–222

Kharaka YK, Maest AS, Carothers WW, Law LM, Lamothe PJ, Fries TL (1987) Geochemistry of metal-rich brines from central Mississippi Salt Dome basin, U.S.A. Appl Geochem 2:534–561

Leach DL, Sangster DF (1993) Mississippi Valley-type lead-zinc deposits. Geological Association of Canada Special Paper 40, pp 289–314

Leach DL, Sangster DF, Kelley KD, Large RR, Garven G, Allen CR, Gutzmer J, Walters S (2005) Sediment-hosted lead–zinc deposits: a global perspective. Econ Geol 100th Anniv:561–607

Li C-Y (1999) Some geological characteristics of concentrated distribution area of epithermal deposits in China. Earth Sci Front (China University of Geosciences, Beijing) 6(1):163–170, in Chinese with English abstract

Liu T-G, Ye L (2000) Geological–geochemical characteristics of Niujiaotang independent cadmium deposit. Acta Mineral Sinica 20(3):279–285 (in Chinese with English abstract)

Liu Y-J, Cao L-M, Li Z-L, Wang H-N, Chu T-Q, Zhang J-R (1984) Geochemistry of individual elements. Science, Beijing, 548 pp (in Chinese)

Liu T-G, Zhang Q, Ye L, Shao S-X (2004a) Discovery of the complete isomorphous series of ZnS–CdS in nature and its preliminary study. Geology China 31(1):40–45 (in Chinese with English abstract)

Liu T-G, Zhang Q, Ye L, Shao S-X (2004b) Discovery of primary greenockite in nature, as exemplified by the Niujiaotang cadmium–zinc deposit, Guizhou. Acta Mineralogica Sinica 24(2):191–196 (in Chinese with English abstract)

Liu J-S, Ma C-Q, Wang S-M, Chen L, Li M (2009) Discovery of solid bitumen inclusions in authigenic rock crystals in Majiang Paleo-oil reservoir and its geological significance. Geol Sci Tech Inform 28 (6):39–44, 50 (in Chinese with English abstract)

Maurel C (1978) Stabilité de la blende dans le système Zn–Cd–S. Bull Mineral 101:406–411

Nathan Y, Soudry D, Levy Y, Shitrit D, Dorfman E (1977) Geochemistry of cadmium in the Negev phosphorites. Chem Geol 142:87–107

Ohmoto H (1972) Systematics of sulfur and carbon isotopes in hydrothermal ore deposits. Econ Geol 67:551–579

Ohmoto H, Rye RO (1979) Isotopes of sulfur and carbon. In: Barnes HL (ed) Geochemistry of hydrothermal ore deposits, 2nd edn. Wiley, New York, pp 509–567

Pan J-Y, Zhang Q, Ri Z-Y (1993) Trace elements in major ore minerals, Caijiaying lead–zinc deposit, Hebei. J Guilin Metallurg Geol Inst 13:386–393 (in Chinese)

Pan Z-P, Ye L, Zhong H, Liu T-G Li C-Y, Cheng Z-T (2008) The pollution characteristics of water during mining in cadmium-rich Pb–Zn ore area as exemplified by the Niujiaotang Cd-rich zinc deposit, Duyun, Guizhou Province. Acta Mineral Sinica 28:401–406 (in Chinese with English abstract)

Pattrick RAD (1978) Microprobe analyses of cadmium-rich tetrahedrites from Tyndrum, Perthshire, Scotland. Mineral Mag 42:286–288

Pattrick RAD, Hall AJ (1983) Silver substitution into synthetic zinc, cadmium, and iron tetrahedrites. Mineral Mag 47:441–451

Pattrick RAD, Mosselmans JFW, Charnock JM (1998) An X-ray absorption study of doped sphalerites. Eur J Mineral 10:239–249

Piatak NM, Seal RR II, Hammarstrom JM (2004) Environmental significance of cadmium and other trace-element concentrations in sphalerite from mineral deposits. Geol Soc Amer Abstr Progr 36(5):27

Pu X-C, Zhou H-D, Wang X-L (1993) Precambrian lithofaces palaeogeography and mineralization in south China. Geology, Beijing, p 191, in Chinese

Rickard DT, Willden M, Mårde Y, Ryhage R (1975) Hydrocarbons associated with lead–zinc ores at Laisvall, Sweden. Nature 225:131–132

Roedder E (1972) The composition of fluid inclusions. US Geol Surv Prof Paper 400:164

Roedder E (1984) Fluid inclusions. Rev Mineral 12:644

Roedder E, Ingram B, Hall WE (1963) Studies of fluid inclusions III. Extraction and quantitative analysis of inclusions in the milligram range. Econ Geol 58:353–374

Rudnick RL, Gao S (2005) Composition of the continental crust. In: Rudnick RL (ed) The crust. Treatise on geochemistry 3. Elsevier, Amsterdam, pp 1–64

Rui Z-Y, Li N, Wang L-S (1991) Mineralization of basinal brine and lead isotopic targeting in Guanmengshan Pb–Zn deposit. Geology, Beijing, p 208 (in Chinese with English abstract)

Saunders JA, Swann CT (1990) Trace-metal content of Mississippi oil field brines. J Geochem Explor 37:171–183

Schaefer MO, Gutzmer J, Beukes NJ, Greyling LN (2004) Mineral chemistry of sphalerite and galena from Pb–Zn mineralization hosted by the Transvaal Supergroup in Griqualand West, South Africa. S Afr J Geol 107:341–354

Schwartz MO (2000) Cadmium in zinc deposits: economic geology of a polluting element. Internat Geol Rev 42:445–469

Surdam RC, Crossey LJ, Hagen ES, Heasler HP (1989) Organic–inorganic interactions and stone diagenesis. AAPG Bull 73:1–23

Sverjensky DA (1984) Oil field brines as ore-forming solutions. Econ Geol 79:23–37

Szymanski JT (1978) The crystal structure of cernyite, Cu_2CdSnS_4, a cadmium analogue of stannite. Can Mineral 16:147–151

Tauson VL, Chernyshev LV (1977) Phase relationships and structural features of ZnS–CdS mixed crystals. Geochem Internat 14:11–22

Tolcin AC (2008) Cadmium. In: Metals and minerals. U.S. Geol Surv Minerals Yearbook 2007 I, pp 15.1–15.9

Tu G-C, Gao Z-M, Hu R-Z, Zhang Q, Li C-Y, Zhao Z-H, Zhang B-G (2003) Geochemistry and mineralization mechanism of dispersed elements. Geology, Beijing, p 424 (in Chinese)

Vasil'yev VI (1966) Saukovite, a new zinc- and cadmium-bearing sulfide of mercury. Acad Sci USSR Dokl Earth Sci Sect 168:123–127

Viets JG, Hopkins RT, Miller BM (1992) Variation in minor and trace metals in sphalerite from Mississippi Valley-type deposits of the Ozark Region: genetic implications. Econ Geol 87:1897–1905

Vlassopoulos D, Wood SA, Mucci A (1990) Gold speciation in natural water: II—the importance of organic complexing experiments with some simple model ligands. Geochim Cosmochim Acta 54:1575–1586

Wagner T, Cook NJ (1998) Sphalerite remobilization during multi-stage hydrothermal mineralization events—examples from siderite–

Pb–Zn–Cu–Sb veins, Rheinisches Schiefergebirge, Germany. Mineral Petrol 63:223–241

Wang H-Y (1993) Geochemical characteristics of lead–zinc deposit in Guizhou. Geology Guizhou 10:274–289 (in Chinese)

Wang H-Y (1996) Regularities and mode of genesis of lead–zinc mineralizations in eastern Guizhou. Guizou Geology 13:72–89 (in Chinese)

Wang H-Y, Shi J-X (1997) Sources of ore-forming materials and controls over depositional differentiation in the epithermal mineralization series in the Danzhai–Sandu–Duyun area of Guizhou province. Acta Mineral Sinica 17:491–500 (in Chinese with English abstract)

Wilkinson JJ, Eyre SL (2005) Ore-forming processes in Irish-type carbonate-hosted Zn–Pb deposits: evidence from mineralogy, chemistry, and isotopic composition of sulfides at the Lisheen Mine. Econ Geol 100:63–86

Xiang C-F, Tang L-J, Jin Z-J, Li R-F, Wang P-W, Dong L (2008) Outcrop sequence stratigraphy of Majiang ancient oil reservoir and its suggestion to the study on the sealing capability of the marine oil field developed in the South China. Acta Geologica Sinica 82(3):346–352 (in Chinese with English abstract)

Ye L (2005) Origin of mineralizing fluid of Niujiaotang Cd-rich zinc deposit, Duyun, Guizhou, China. Geochim Cosmochim Acta 69: A851

Ye L, Liu T-G (1997) A preliminary discussion on cadmium resource of Duyun area, Guizhou and its prospect. Guizhou Geology 14 (2):160–163 (in Chinese with English abstract)

Ye L, Liu T-G (1999) Sphalerite chemistry. Niujiaotang Cd-rich zinc deposit, Guizhou, Southwest China. J Geochem 18:62–68

Ye L-J, Chen Q-Y, Li R-W (1998) The mineralization of biological organic and its mineralization background. Ocean, Beijing, p 462 (in Chinese)

Ye L, Pan Z-P, Li C-Y, Liu T-G, Xia B (2005) Isotopic geochemical characters in Niujiaotang Cd rich zinc deposit, Duyun, Guizhou. J Mineral Petrol 25:70–74 (in Chinese with English abstract)

Ye L, Pan Z-P, Li C-Y, Liu T-G (2006) The environmental effect of cadmium-rich Pb–Zn deposit, as exemplified by Niujiaotang Cd-rich Zn deposit, Guizhou, China. Chinese J Geochem 25 (Suppl):45

Ye L, Cook NJ, Ciobanu CL, Liu Y-P, Zhang Q, Liu T-G, Gao W, Yang Y-L, Danyushevsky L (2011) Trace and minor elements in sphalerite from base metal deposits in South China: a LA-ICPMS study. Ore Geol Rev 39:188–217

Yushkin NP, Yeremin NI, Koroshilova LA (1975) New manganiferous variety of sphalerite. Doklady Akad Nauk SSSR 216:166–169

Zartman RE, Doe BR (1981) Plumbotectonics—the model. Tectonophysics 75:135–162

Zhang A-Y (1987a) The geochemistry of marine black rock series and its metallogenic significance. Science, Beijing, p 240, in Chinese

Zhang Q (1987b) Trace elements in galena and sphalerite and their geochemical significance in distinguishing in genetic types of Pb–Zn ore deposits. Chinese J Geochem 6(2):177–190

Zhang B-Z, Qin M, Li M-D (1994) Mineralization conditions and genesis, Niujiaotang zinc orefield, Duyun. Guizhou Geology 11 (4):287–293 (in Chinese)

Zhao K-D, Jiang S-Y, Jiang Y-H, Wang R-C (2005) Mineral chemistry of the Qitianling Granitoid and the Furong tin ore deposit in Hunan Province, South China: implication for the genesis of granite and related tin mineralization. Eur J Mineral 17:635–648